Optical concept of a compressor for XUV pulses in the attosecond domain

Fabio Frassetto, Paolo Villoresi and Luca Poletto

CNR/INFM Laboratory for Ultraviolet and X-Ray Optical Research
Department of Information Engineering, University of Padova
Via Gradenigo 6/b, 35131 Padova, Italy
Corresponding author: poletto@dei.unipd.it

Abstract: We discuss the phase properties of a double-grating compressor with grazing-incidence gratings in the off-plane mount, designed for the temporal compression of XUV attosecond pulses produced with the technique of high-order harmonic generation. Its purpose is to introduce a negative chirp that compensates for the intrinsic chirp of the pulse. The study is based on the path lengths of the rays at different wavelengths, and their control in order to achieve either positive or negative group-delay dispersion. We demonstrate that the sign and the amount of the dispersion introduced is controlled by a linear translation of a grating. Beside the instrument is expected to present a high throughput, constant along the spectrum of interest. The compressor can be designed for any spectral region in the XUV and soft X-ray domain. As a test case, the applications to the compression of attosecond pulses centered at 70 eV and at 160 eV are discussed.

OCIS codes: 190.4160 Multiharmonic generation; 320.0320 Ultrafast optics; 050.1950 Diffraction gratings; 050.1960 Diffraction theory.

References and links

1. P. Jaegle', *Coherent Sources of XUV Radiation* (Springer, Berlin, 2006).
2. M. Hentschel, R. Kienberger, Ch. Spielmann, G. A. Reider, N. Milosevic, T. Brabec, P. Corkum, U. Heinzmann, M. Drescher, and F. Krausz, "Attosecond metrology," Nature **414**, 509-513 (2001).
3. R. Kienberger, M. Hentschel, M. Uiberacker, Ch. Spielmann, M. Kitzler, A. Scrinzi, M. Wieland, Th. Westerwalbesloh, U. Kleineberg, U. Heinzmann, M. Drescher, and F. Krausz, "Steering Attosecond Electron Wave Packets with Light," Science **297**, 1144-1148 (2002).
4. A. Baltuska, T. Udem, M. Uiberacker, M. Hentschel, E. Goulielmakis, C. Gohle, R. Holzwarth, V. Yakovlev, A. Scrinzi, T. Hansch, and F. Krausz, "Attosecond control of electronic processes by intense light fields," Nature **421**, 611-615 (2003).
5. H. Niikura, D. M. Villeneuve, and P. B. Corkum, "Mapping Attosecond Electron Wave Packet Motion," Phys. Rev. Lett. **94**, 083003 (2005).
6. P. B. Corkum and F. Krausz, "Attosecond science," Nature Physics **3**, 381-387 (2007).
7. P. M. Paul, E. S. Toma, P. Breger, G. Mullot, F. Auge, Ph. Balcou, H. G. Muller, and P. Agostini, "Observation of a train of attosecond pulses from high harmonic generation," Science **292**, 1689-1692 (2001).
8. R. Lopez-Martens, K. Varju, P. Johnsson, J. Mauritsson, Y. Mairesse, P. Salières, M. B. Gaarde, K. J. Schafer, A. Persson, S. Svanberg, C.-G. Wahlström, and A. L'Huillier, "Amplitude and phase control of attosecond light pulses," Phys. Rev. Lett. **94**, 033001 (2005).
9. R. Kienberger, E. Goulielmakis, M. Uiberacker, A. Baltuska, V. Yakovlev, F. Bammer, A. Scrinzi, Th. Westerwalbesloh, U. Kleineberg, U. Heinzmann, M. Drescher, and F. Krausz, "Atomic transient recorder," Nature **427**, 817 (2004).
10. M. Schultze, E. Goulielmakis, M. Uiberacker, M. Hofstetter, J. Kim, D. Kim, F. Krausz, and U. Kleineberg, "Powerful 170-attosecond XUV pulses generated with few-cycle laser pulses and broadband multilayer optics", New J. Phys. **9** 243-253 (2007).

#92254 - $15.00 USD Received 29 Jan 2008; revised 17 Mar 2008; accepted 21 Mar 2008; published 25 Apr 2008

11. J. Sola, E. Mevel, L. Elouga1, E. Constant, V. Strelkov, L. Poletto, P. Villoresi, E. Benedetti, J.-P. Caumes, S. Stagira, C. Vozzi, G. Sansone, and M. Nisoli, "Controlling attosecond electron dynamics by phase-stabilized polarization gating," Nature Phys. **2**, 319 (2006).
12. G. Sansone, E. Benedetti, F. Calegari, C. Vozzi, L. Avaldi, R. Flammini, L. Poletto, P. Villoresi, C. Altucci, R. Velotta, S. Stagira, S. De Silvestri, and M. Nisoli, "Isolated single-cycle attosecond pulses," Science **314**, 443-446 (2006).
13. P. Tzallas, E. Skantzakis, C. Kalpouzos, E. P. Benis, G. D. Tsakiris, and D. Charalambidis, "Generation of intense continuum extreme-ultraviolet radiation by many-cycle laser fields", Nature Phys. **3**, 846-850 (2007).
14. L. Poletto and P. Villoresi, "Time-compensated monochromator in the off-plane mount for extreme-ultraviolet ultrashort pulses," Appl. Opt. **45**, 8577-8585 (2006).
15. P. Villoresi, "Compensation of optical path lengths in extreme-ultraviolet and soft-x-ray monochromators for ultrafast pulses," Appl. Opt. **38**, 6040-6049 (1999).
16. O. Martinez, "3000 times grating compressor with positive group velocity dispersion: Application to fiber compensation in 1.3-1.6 μm region," IEEE J. Quantum Electron. **23**, 59-64 (1987)
17. O. Martinez, "Design of high-power ultrashort pulse amplifiers by expansion and recompression," IEEE J. Quantum Electron. **23**, 1385-1387 (1987).
18. I. Walmsley, L. Waxer, and C. Dorrer, "The role of dispersion in ultrafast optics," Rev. Sci. Instrum. **72**, 1-28 (2001).
19. L. Poletto, "Time-compensated grazing-incidence monochromator for extreme-ultraviolet and soft X-ray high-order harmonics," Appl. Phys. B **78**, 1013-1016 (2004).
20. L. Poletto, P. Villoresi, E. Benedetti, F. Ferrari, S. Stagira, G. Sansone, and M. Nisoli, "Intense femtosecond extreme ultraviolet pulses by using a time-delay compensated monochromator," Opt. Lett. **32**, 2897-2899 (2007).
21. W. Cash, "Echelle spectrographs at grazing incidence," Appl. Opt. **21**, 710–717 (1982).
22. M. Nevière in *Electromagnetic Theory of Grating* (cap. IV), R. Petit ed. (Springer-Verlag, 1980).
23. W. Cash and R. Kohnert, "Very high X-ray efficiency from a blazed grating," Appl. Opt. **21**, 17-18 (1982).
24. J. F. Seely, L. I. Goray, B. Kjornrattanawanich, J. M. Laming, G. E. Holland, K. A. Flanagan, R. K. Heilmann, C.-H. Chang, M. L. Schattenburg, and A. P. Rasmussen, "Efficiency of a grazing-incidence off-plane grating in the soft-x-ray region," Appl. Opt. **45**, 1680-1687 (2006).
25. L. Poletto, S. Bonora, M. Pascolini, F. Borgatti, B. Doyle, A. Giglia, N. Mahne, M. Pedio, and S. Nannarone, "Efficiency of gratings in the conical diffraction mounting for an EUV time-compensated monochromator," Proc. SPIE **5534**, 144–153 (2004).
26. M. Pascolini, S. Bonora, A. Giglia, N. Mahne, S. Nannarone, and L. Poletto, "Gratings in the conical diffraction mounting for an EUV time-delay compensated monochromator," Appl. Opt. **45**, 3253-3562 (2006).
27. L. Poletto, S. Bonora, M. Pascolini, and P. Villoresi, "Time-frequency analysis of single-shot high-order harmonic spectra," Rev. Sci. Instrum. **75**, 4413-4418 (2004).
28. V. Ayvazyan et al, "Operation of a Free Electron Laser in the Wavelength Range from the Extreme Ultraviolet to the Water Window," Nature Photonics **1**, 336-342 (2007).

1. Introduction

High-order harmonics (HHs) generated by the interaction between an ultra-short laser pulse and a gas jet are considered as a very relevant source of coherent extreme-ultraviolet (XUV) and soft X-ray radiation of very short time duration and high peak brilliance, with important applications in several areas both in fundamental research and in advanced technology [1]. The HH spectrum is described as a sequence of peaks corresponding to the odd harmonics of the fundamental laser wavelength and having an intensity distribution characterized by a vast plateau, whose extension is related to the pulse intensity. The radiation generated with the scheme of the HHs generated by laser pulses of a few optical cycles recently become the tool for the investigation of matter with sub-femtosecond, or attosecond, resolution (1 as = 10^{-18} s) [2-5]. The access to this unexplored time domain opens new frontiers in atomic, molecular and solid-state science [6], as it becomes possible to do experiments with an unprecedented time resolution and intensity.

The understanding of the atomic phenomena which give birth to the attosecond pulses has been exploited in the past few years to demonstrate experimentally the generation of either trains [7,8] as well as isolated [9-12] bursts of attosecond radiation. The physical grounds of

#92254 - $15.00 USD Received 29 Jan 2008; revised 17 Mar 2008; accepted 21 Mar 2008; published 25 Apr 2008

such short pulses originate from the model of HHs generation, i.e. the phase-matched emission of radiation as result of the recombination of a photoionized electron with its parent ion. Once the conditions for such recombination are realized in only one occurrence per laser pulse, an isolated ultrashort XUV pulse is generated.

Two techniques have so far demonstrated the generation of isolated attosecond pulses. The first is based on the selection of a single active quantum path responsible for the emission of the high energy portion of the HHs spectrum [2] that has recently achieved the lowest value of 170 as [10]. The other is based on the polarization gating technique and exploits the continuously varying ellipticity of the pump pulse so to select a single active quantum path for the photoelectrons for an extended portion of the emitted spectrum that reached the lower value of 130 as [12]. The proposal of the generation with many cycle intense pulses was also recently presented [13]. In both cases, the pulses are positively chirped, as resulting from the different duration of the quantum paths that contribute to different portion of the emitted spectrum. Also attosecond pulses generated in a train exhibit an intrinsic positive chirp [7] so their temporal duration is longer than the Fourier limit.

Positively chirped pulses may be temporally compressed down to the Fourier limit by introducing a system that gives a negative chirp that compensates for the intrinsic chirp of the pulse. This problem has been successfully addressed by exploiting the negative Group-Delay Dispersion (GDD) of a thin metallic filter [8,12]. In particular, the compression suitable for the pulse was obtained using a 300 nm thick aluminum foil. Compression using metallic filter is very simple and effective, but has some remarkable drawbacks. First of all, the absorption of the filter may be significant, exceeding one order of magnitude. Furthermore, since the amount of GDD introduced by the filter depends on its thickness, the system throughput depends also on the compression properties. Most of all, this compression technique has some rigid limitations in the choice and extent of the energy region, as the compression properties derive from the elemental properties of the foil. As an example, by using the polarization gating technique with neon as a target atom, the generation of pulses with larger spectrum, which support sub-100 as pulses at an energy around 45 eV has been reported [11], but not compressed so far for lacks of suitable filter elements.

We present here a method that aims to solve the problem of temporal compression of broad-band XUV attosecond pulses by exploiting the influence on the pulse phase of a double-grating compressor. The design of the XUV attosecond Compressor (XAC) originates from the scheme of an XUV time-delay compensated monochromator (TCM) realized to select a suitable portion of the HHs spectrum within a broad spectral interval without altering the intrinsic femtosecond pulse time duration [14]. The TCM scheme adopts a double-grating configuration which compensates for the temporal stretching of the pulse imparted by a single diffraction grating [15]. This effect follows from the principle of grating diffraction, in which the optical paths followed by rays diffracted by nearby grooves differ of multiples of the wavelength in order to realize constructive interference. The introduction of a double-grating design in which the second grating compensates for the dispersion of the optical paths of rays given by the first grating allows to realize a so called time-delay compensated instrument, in which all the rays emitted by the source at the same wavelength make the same optical paths. This principle is used in many ultrafast devices in the visible and near infrared, as it was demonstrated that grating pairs may be arranged to realize compensators for the laser cavity dispersion, phase modulators, stretchers and compressors for chirped pulse amplification [16-18]. Nevertheless, their use as a compressor has never been considered so far for the very delicate case of the XUV attosecond pulses. In fact, the correction of the optical path has to be controlled with a precision of few tens of nanometers, over a bandwidth of about an octave.

The TCM designs based on the use of grazing-incidence gratings in the classical diffraction mounting [15] suffers from low throughput and a narrow region of tunability. A remarkable improvement both in throughput and tunability in the XUV has been demonstrated by exploiting the off-plane mount of gratings [19], that differs from the classical mount in that

#92254 - $15.00 USD Received 29 Jan 2008; revised 17 Mar 2008; accepted 21 Mar 2008; published 25 Apr 2008

the incident and diffracted wave vectors are almost parallel to the grating grooves. By using a TCM instrument with two gratings in the off-plane mount, the production of intense monochromatized and ultrashort XUV pulses has been recently demonstrated [20], confirming the validity of the time-delay compensated optical design.

The XAC scheme here presented is able to introduce either a positive or negative GDD in a broad band. By choosing a suitable pair of gratings, it can be operated in any spectral interval within the XUV and soft X-ray regions (10-300 eV). In addition, the photon throughput is higher than that of a conventional two-grating configuration and does not vary with the amount of GDD that is introduced.

The geometry of the off-plane mount and the optical scheme of the compressor are presented respectively in Par. 2 and 3. The phase properties of the instrument are discussed in Par. 4. As test cases, the applications to the compression of attosecond pulses centered at 70 eV and at 160 eV are presented in Par. 5 and 6.

2. The off-plane mount

The off-plane mount of diffraction gratings differs from the classical one in that the incident and diffracted wave vectors are almost parallel to the grating grooves [21]. The geometry is shown in Fig. 1. The direction of the incoming rays is described by two parameters, the altitude and the azimuth. The altitude γ is the angle between the direction of the incoming rays and the direction of the grooves. It defines the half-angle of the cone into which the light is diffracted: all the rays leave the grating at the same altitude angle at which they approach. The azimuth α of the incoming rays is defined to be zero if they lie in the plane perpendicular to the grating surface and parallel to the rulings. Let β define the azimuth of the diffracted light at wavelength λ and order *m*. The grating equation is written as

$$\sin\gamma(\sin\alpha+\sin\beta)=m\lambda\sigma\,, \tag{1}$$

where σ is the groove density.

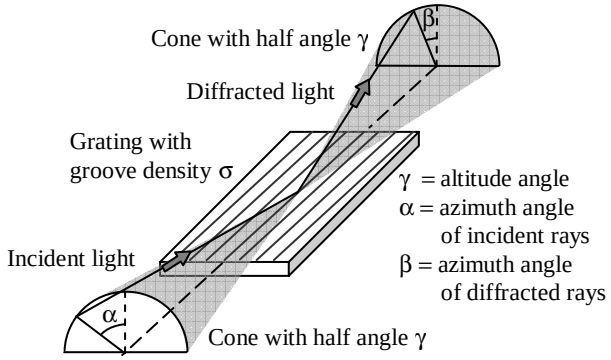

Fig. 1. Geometry of the off-plane mount for a plane diffraction grating.

It has been theoretically shown and experimentally measured that the efficiency in the off-plane mount is close to the reflectivity of the coating [22-26], so much higher efficiencies than in the classical diffraction mount can be obtained in the XUV. The blaze condition of maximum efficiency is verified when the light leaves the grating in such a way that it performs a specular reflection on the groove surface, that is $\alpha + \beta = 2\delta$, where δ is the grating blaze angle, i.e. the inclination of the facets of the grooves with respect to the grating surface. In addition, shadowing effects from adjacent grooves must be avoided, that is $\alpha = \delta$. It follows that the highest efficiency of a blaze grating in the off-plane mount is achieved when $\alpha = \beta = \delta$: it indicates that each groove of the grating is seen by the incident ray as a portion of

#92254 - $15.00 USD Received 29 Jan 2008; revised 17 Mar 2008; accepted 21 Mar 2008; published 25 Apr 2008

a plane mirror. The corresponding blaze wavelength is $\lambda_B = 2 \sin\gamma \sin\delta/m\sigma$. In view of the application to TCM schemes, the efficiency of gratings in the off-plane mount has been previously measured and it has been demonstrated that efficiencies substantially higher than those of the classical diffraction scheme are supported in a bandwidth of more than one octave in the XUV [26].

3. Optical scheme of the compressor

The optical scheme of the attosecond compressor is shown in Fig. 2. The layout consists of four grazing-incidence parabolic mirrors, indicated as P1, P2, P3 and P4, and two plane gratings operated in the off-plane mount, indicated as G1 and G2. The compressor is divided in two equal sections, each of them with two parabolic mirrors and a plane grating (P1-G1-P2 and P3-G2-P4). The schematic is similar to the TCM design in the off-plane mount [14], although it differs for the use of the parabolic mirrors instead of the toroidal ones and the absence of the intermediate slit.

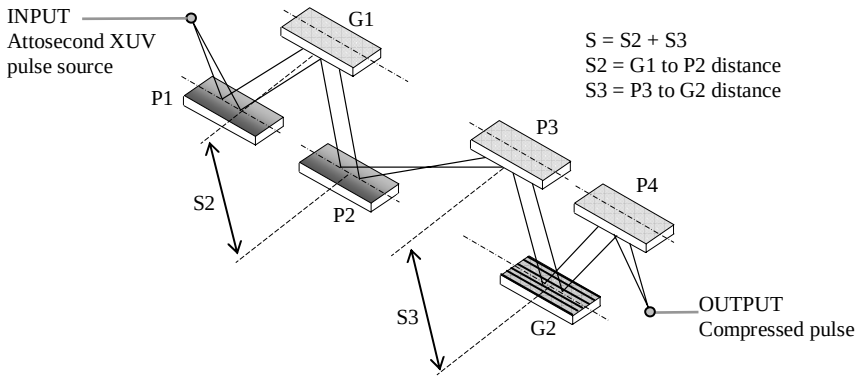

Fig. 2. Layout of the XUV attosecond compressor.

The source of the attosecond input beam whose chirp has to be corrected is located at the front focal distance of the first mirror P1. The first section gives a spectrally dispersed image of the source on the intermediate plane.

Since the gratings have to be operated in parallel light, the first mirror of each of the two sections acts as the collimator and the second mirror as the focusing element. The four mirrors are operated at equal grazing angle and unity magnification, i.e. the input arm of each of the two collimators is equal to the output arm of each of the two focusing elements. With reference to Fig. 2, the term "*input arm*" refers to the two collimators P1 and P3 and indicates the distance between the source and the center of P1 or the distance between the intermediate focal point and the center of P3; the term "*output arm*" refers to the two focusing elements P2 and P4 and indicates the distance between the center of P2 and the intermediate focal point or the distance between the center of P4 and the output focal point. The focal length f_1, f_2, f_3, f_4 of the four mirrors are chosen by

$$f_i = p_i \sin^2\theta, \quad i = 1,2,3,4 \tag{2}$$

where θ is the grazing angle on the mirrors, that is assumed to be the same for all the optics, p_1 and p_3 are the input arms of P1 and P3, p_2 and p_4 are the output arms of P2 and P4. For the time-delay compensation, the number of grooves illuminated on G2 has to be equal to that on G1 and this requires that P2 and P3 have the same arms, i.e. $p_2 = p_3 = p''$. The total

#92254 - $15.00 USD Received 29 Jan 2008; revised 17 Mar 2008; accepted 21 Mar 2008; published 25 Apr 2008

magnification of the instrument is $M = (p_2/ p_1)\cdot(p_4/ p_3) = p_4/ p_1$. In the following, we will assume to have unity magnification, that is $p_1 = p_4 = p'$.

The use of parabolic mirrors instead of the more simple toroidal ones adopted for the original TCM scheme is required to reduce the aberrations of the optical system, in fact any aberration causes a spread of the length of the optical paths of the rays within the aperture of the instrument. Since we want to compress pulses in the few-tens attosecond time scale, an unprecedented correction of the aberrations is required. For a grazing-incidence system to be used in the XUV this constraint imposes the use of an advanced optical design. The ideal collimator of the rays emitted by a point source is a paraboloidal surface; this is also the ideal focusing element, completely free from aberrations in case of a point-like source. It will be shown by simulations that toroidal surfaces at grazing incidence show residual aberrations that are intolerable in the attosecond time scale. Only paraboloidal surfaces show acceptable optical performances when used in grazing incidence.

To fulfill the compensation of the optical paths, the gratings G1 and G2 have to be equal with same groove density and blaze angle. Furthermore, they have to be operated at the same altitude angle. Different pairs of gratings have to be used for different spectral intervals.

After the reflection on P1, the beam is collimated and propagates toward G1, whose center is placed at a distance S1 from the center of P1 and S2 from the center of P2. The azimuth angle α_1 of the incident rays on G1 is the same for all the wavelengths and gives the wavelength of maximum diffraction efficiency $\lambda_B = 2 \sin\gamma \sin\delta/\sigma$ with $\beta_1(\lambda_B) = \alpha_1 = \delta$. The azimuth angle $\beta_1(\lambda)$ of the rays diffracted from G1 at different wavelengths is calculated from Eq. (1). The diffracted radiation is collected by P2, which realizes a spectrally disperse image of the source on its focal plane. This is the source plane for the second section of the compressor. Again, after the reflection on P3, the beam is collimated and propagates toward G2, whose center is placed at a distance S3 from the center of P3 and S4 from the center of P4. Due to the symmetry of the configuration, the azimuth angle $\alpha_2(\lambda)$ of incident rays on G2 is equal to the azimuth angle $\beta_1(\lambda)$. Since the gratings are equal and operated at the same altitude angle, the azimuth angle β_2 of the rays diffracted from G2 is constant with the wavelength and equal to α_1, so all the exit rays are parallel. The rays are finally focused on the output focal point by P4.

The two-grating design of a TMC requires the two following characteristics: 1) the differences in the path lengths of rays with the same wavelength but with different entrance directions within the beam aperture that are caused by the first grating are compensated by the second grating, and 2) two rays at different wavelengths within the spectrum of the pulse to be selected are focused on the same output point, as discussed in detail in [14].

In the actual XAC design we consider that the rays with different wavelengths are diffracted by G1 at different azimuth angles. Thus they do not make the same optical path within the instrument. The group delay (GD), intended here as the propagation time of the rays from the source point to the output focal point, depends then on the wavelength. We analyze here the GDD introduced by the compressor to calculate analytically its sign and amount. Since all the rays are collimated in the paths S1 between P1 and G1 and S4 between G2 and P4, it is clear that the variations of the optical paths with the wavelength do not depend from the choice of S1 and S4, that can be arbitrarily selected.

Once the arm p'' of P2 and P3 and the grating parameters have been selected, the variation of the group delay depends only by the choice of the distances S2 and S3, in particular it will be shown that it depends by their sum S2 + S3 = S. This is the only parameter to be properly set to introduce the required variation of the group delay, then the required GDD.

Due to the symmetry of the configuration, G1 is imaged on G2 when $S = 2p''$. This is the condition for having the group delay constant with the wavelength, i.e. GDD = 0. For $S < 2p''$, G1 is imaged behind G2 and the resulting GDD is positive. For $S > 2p''$, G1 is imaged before

#92254 - $15.00 USD Received 29 Jan 2008; revised 17 Mar 2008; accepted 21 Mar 2008; published 25 Apr 2008

G2 and the resulting GDD is negative. Therefore, the amount of GDD introduced depends on S and not by the individual distances S2 and S3.

The mechanical design is simplified if S1 is maintained fixed and S2 is finely tuned to change the GDD. The variation of S2 is performed by mounting G2 on a linear translator and moving it along an axis coincident with the straight line which connects the centers of P3 and G2, as illustrated in Fig. 3.

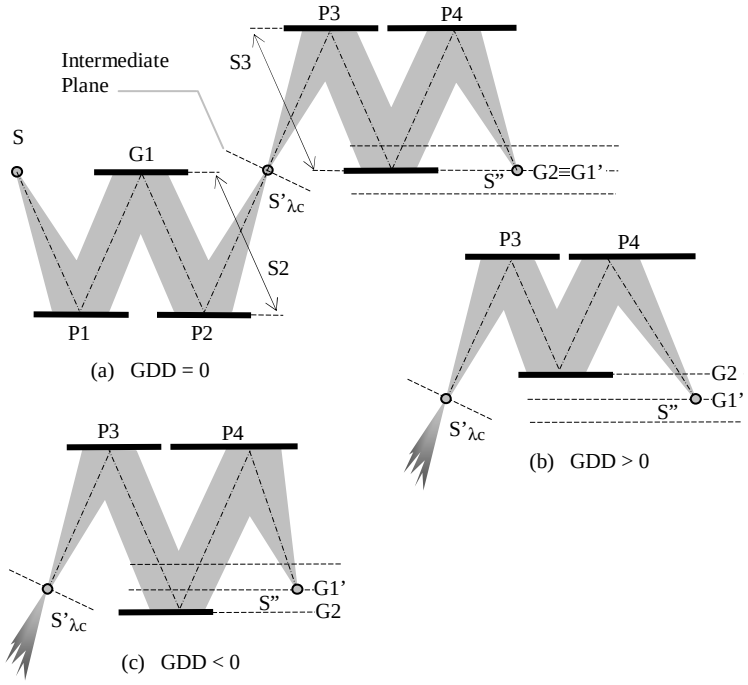

Fig. 3. XAC operation as a compressor and as a stretcher. The setup make use of two plane gratings G1 and G2, two collimators, and two condenser elements. a) GDD equal to zero; b) positive GDD: c) negative GDD.

Since all the wavelengths are diffracted from G2 in a collimated beam with constant direction, P4 is maintained fixed and the radiation is focused always on the same output focal point. The variation of S3 implies a variation also of S4, but this does not influence the GDD. The size of mirror P4 has to be slightly larger than the other three mirrors due to the displacement of the beam on the mirror surface. From the geometrical point of view, the compressor has fixed input and output points, fixed output direction and a single mechanical movement to finely tune the GDD. The properties of the compressor are resumed in Tab. 1.

#92254 - $15.00 USD Received 29 Jan 2008; revised 17 Mar 2008; accepted 21 Mar 2008; published 25 Apr 2008

Tab. 1. XAC optical parameters.

Mirrors	**Paraboloidal:** P1, P2, P3 P4
Input/output arms	p_i i = 1,2,3,4
	$p_1 = p_4 = p'$
	$p_2 = p_3 = p''$
Grazing angle	θ
Gratings	**Plane:** G1, G2
Groove density	σ
Altitude angle	γ
Blaze angle	δ
Distances	
P1-G1	S1
G1-P2	S2
P3-G2	S3
G2-P4	S4
GDD	
S = S2 + S3=$2p''$	GDD = 0
S = S2 + S3 < $2p''$	GDD > 0
S = S2 + S3 > $2p''$	GDD < 0

4. Phase properties of the compressor

The modeling of the compressor is done with a ray-tracing program written by the authors and able to calculate the length of the optical paths OP(ω) of the rays propagating in the instrument, where the dependence of OP from the angular frequency $\omega = 2\pi c/\lambda$ is explicitly indicated. Here c is the light velocity in vacuum and λ the wavelength.

Once OP(ω) has been calculated, the group delay GD(ω) is given as

$$GD(\omega) = \frac{OP(\omega)}{c}. \tag{3}$$

The group delay is numerically calculated by the ray-tracing program for different values of the distance S. The results are then fitted by a polynomial expression in ω, to a given order N:

$$GD(\omega) = t_0 + \frac{(2p''-S)}{c} \sum_{i=0}^{N} a_i (\omega - \omega_c)^i , \tag{4}$$

where t_0 is the constant group delay for $S = 2p''$, i.e. $t_0 = (2p' + 4p'' + S_1 + S_4)/c$, and ω_c is the central frequency $\omega_c=(\omega_{max} + \omega_{min})/2$, with ω_{max} and ω_{min} respectively the maximum and the minimum frequency in the pulse spectral band. The variation of the group delay at a fixed frequency is here assumed to be linear with S. The results of the simulations indicate that this assumption is well verified, as explained later in Par. 5.2.

The Group Delay Dispersion and the Third Order Dispersion (TOD) are then defined respectively as the derivatives of the group delay and of the GDD with respect to the frequency:

$$GDD(\omega) = \frac{\partial GD(\omega)}{\partial \omega} = \frac{(2p''-S)}{c} \sum_{i=1}^{N} a_i i (\omega - \omega_c)^{i-1} \tag{5}$$

$$TOD(\omega) = \frac{\partial GDD(\omega)}{\partial \omega} = \frac{\partial^2 GD(\omega)}{\partial \omega^2} = \frac{(2p''-S)}{c} \sum_{i=2}^{N} a_i i(i-1)(\omega - \omega_c)^{i-2} \tag{6}$$

#92254 - $15.00 USD Received 29 Jan 2008; revised 17 Mar 2008; accepted 21 Mar 2008; published 25 Apr 2008

The effects on the phase of the pulse higher than the third order can be analogously calculated from Eq. (4).

As previously said, once the spectral region of operation has been selected, the XUV grating stretcher/compressor can then provide either a positive or a negative dispersion without changing the optical set-up, but simply modifying S by a linear translation of grating G2.

5. Compressor for the 50-100 ev region

The design of a compressor for attosecond pulses in the 50-100 eV (24.8-12.4 nm) region is here presented. The optical parameters are reported in Tab. 2. Note that the thin metallic filters used up to now for compression, that are Al and Zr, cannot be used in this broad spectral region: in fact, the transmission of a thin Al filter is zero in the 72-100 eV region, while the transmission of a thin Zr filter drops down to zero in the 50-60 eV region. On the contrary, the transmission of the grating compressor is expected to be almost constant, due to the use of optics in grazing incidence.

The grazing angle on the mirrors is chosen to be 3°, in order to realize the conditions for high reflectivity in the spectral region of operation. In the case of gold coating, the reflectivity for s-polarized light is about 0.90 in the 50-100 eV region, so the contribution of the mirrors to the total throughput is $0.90^4 = 0.65$. The four mirrors are equal, with arms $p' = p'' = 200$ mm. The acceptance angle is 6 mrad that matches the expected divergence of XUV ultrashort pulses [25]. The resulting size of the illuminated portion of the paraboloidal mirrors is of 23 mm × 1.2 mm, which can be considered quite small for what concern the optical polishing required. A small reflecting area assures a high quality in the finishing of the surface, both in terms of figuring errors and of slope errors. The provision of optical surfaces with errors in the shape lower than 20 nm and slope errors lower than 1 μrad rms is essential to have time-delay compensation in the range of tens of attoseconds. These requirements can be well satisfied by manufacturers on such small areas. The effects of the errors on the surface finishing will be analyzed later.

Tab. 2. Parameters of the XAC for the 50-100 eV spectral region.

Pulse spectral interval	50-100 eV (12.4-24.8 nm)
Mirrors	**Off-axis paraboloidal**
Input/output arms	200 mm
Acceptance angle	6 mrad × 6 mrad
Grazing angle	3°
Size of illuminated area	23 mm × 1.2 mm
Coating	Gold
Gratings	**Plane**
Groove density	200 gr/mm
Altitude angle	1.5°
Blaze angle	4.5°
Size of diffracting area	45 mm (// to the grooves) × 1.2 mm
Coating	Gold
Distances	
S1, S2, S4	50 mm
S3	> 350 mm for negative GDD
Zero-order trap	150 mm far from P2
Intermediate slit	0.5 mm wide
Total length of the compressor	1.3 m

The gratings have 200 gr/mm groove density. They are blazed at 4.5° and are operated at an altitude of 1.5°. The altitude and blaze angles have been selected to optimize the time-delay compensation, as shown in details in the next section. Since the gratings are ruled on plane

#92254 - $15.00 USD Received 29 Jan 2008; revised 17 Mar 2008; accepted 21 Mar 2008; published 25 Apr 2008

substrates and have a small area, the high quality required in the surface finishing is easily obtained by the manufacturers. We assume S2 = 50 mm just to have S1 = S2 = S4. Once *p*" has been fixed, the distance S3 is consequently calculated as explained in Tab. 1.

The IR laser fundamental radiation has to be stopped within the compressor to avoid the propagation of the laser pulse toward the sample to be analyzed. This is performed by a suitable zero-order trap, as an absorbing dark screen, placed between P2 and the intermediate focal point, where different wavelengths are spatially separated. In the case here presented, the trap can be inserted 150 mm far from the center of P2 (i.e. 50 mm far from the intermediate focal point), where the zero-order radiation and the lowest wavelength within the spectral width of the pulse (i.e. 12.4 nm) are spatially separated.

Since the diffraction efficiency of the gratings G1 and G2 at first order is less than unity, a fraction of the incident radiation is diffracted also at the 0^{th} and at higher diffraction orders, although with a very low intensity since the off-plane mount assures high selectivity of the diffracted orders when the azimuth angles are close to the blaze angle [24]. Nevertheless, these rays propagate toward the output and have to be stopped inside the instrument, because they alter the time-delay compensation and also the phase properties of the compressor. For this purpose, a suitable horizontal slit is placed on the intermediate focal point. The width of the slit depends on the extension of the spectral interval of operation and on the wavelength dispersion of the first section and has to be selected to let rays propagate only at the 1^{st} diffracted order. In the case here presented, the width of the intermediate slit is 0.5 mm.

The rays diffracted by G2 at orders different than the 1^{st} one are focused by P4 on the output plane on different heights with respect to the optical axis. They can be stopped, if required, by placing a slit close to the output focal point.

Due to the use of parabolic mirrors, the aberrations of this configuration are negligible. For a point-like source, the aberrations on the focal plane are lower than 0.2 micrometers rms.

The efficiency of gratings in the off-plane mount for time-delay-compensated monochromators has been measured to be as high as 0.5 at 20 nm [26]. Furthemore the TCM presently on operation has a total efficiency of 0.18 at 30 nm [20]. On the basis of these measurements, the total transmission of the compressor is expected to be in the 0.15-0.20 range.

5.1 Time-delay compensation

The time-delay compensation of the compressor has been analyzed by ray-tracing simulations. It has to be verified that the differences in the path lengths of rays with the same wavelength but with different entrance directions within the beam aperture that are caused by the first grating are compensated by the second grating. This indicates that all the rays with the same wavelength emitted by the source within the acceptance angle of the instrument make the same optical path from the input to the output of the compressor.

Once the grating groove density is selected, the time-delay compensation depends from the choice of the altitude and azimuth angles. Both these parameters have to be optimized in order to minimize the residual spreads of the optical paths.

At a fixed altitude angle, the azimuth angle (i.e. the blaze angle of the grating) has to be chosen to have the best time-delay compensation within the whole spectral region of operation. The effect of the azimuth angle on the compensation is illustrated in Fig. 4 for two different altitude angles. The full-width-at-half-maximum (FWHM) spreads of the optical paths as a function of the azimuth angle are shown. The spread is almost zero at the blaze wavelength and increases far from it. This can be explained by the fact that only at the blaze wavelength the chief ray propagates coincident with the optical axis of the compressor, so the time-delay compensation is almost perfect. The optimum azimuth is determined when the maximum residual spread is minimized within the spectral interval of operation: this is achieved when the spread is the same at the two extremes of the interval.

#92254 - $15.00 USD Received 29 Jan 2008; revised 17 Mar 2008; accepted 21 Mar 2008; published 25 Apr 2008

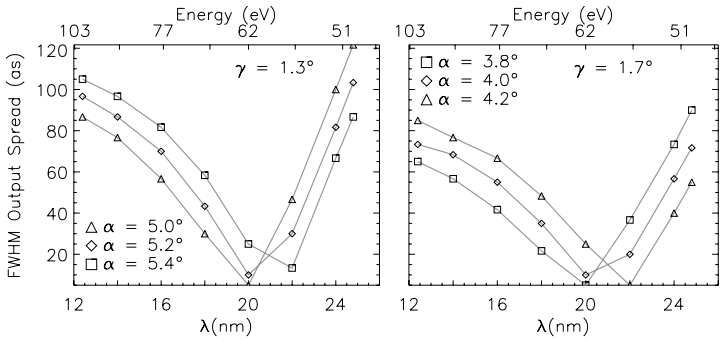

Fig. 4. Analysis of the time-delay compensation of the compressor for the 50-100 eV region. The graphs show the FWHM spreads of the optical paths of rays for two altitude angles and different azimuth angles.

The final parameter to be chosen is then the altitude angle. The spreads as a function of this angle are shown in Fig. 5 both at the intermediate focal plane and at the output plane. For each altitude, the optimum azimuth has been selected as explained in the previous paragraph. The differences in the path lengths, that in the intermediate plane are of several femtoseconds, are almost canceled by the compensated configuration. Furthermore, a correct selection of the altitude angle gives a residual spread of the optical paths of several attoseconds within the whole spectral region of operation. In the design here presented, the optimum altitude is selected to be 1.5°, with a residual spread of less than 10 as FWHM. It has been verified by the simulations that the optimum time-delay compensation is obtained for the altitude angle giving that all the rays at different wavelengths are almost focused on the optical axis of the compressor. In fact, a spread of the positions of the spot sizes at the different wavelengths of even few micrometers in the direction transversal with respect to the optical axis, gives a difference in the length of the optical paths of several tens of attoseconds, which are unacceptable for the application here presented. This is explained in Fig. 6. For a given configurations, it is shown the position of the spot size of the different wavelengths on the focal plane. The better time-delay compensation is obtained when the spots are almost superimposed.

5.2 Phase properties

The results of the calculation of the phase properties of the compressor are resumed in Fig. 7. The group delay is shown in Fig. 7(a1). It has been calculated by the ray-tracing program for different values of the distance S, then it has been fitted by a 4^{th}-order polynomial with the formula given by Eq.(4) where t_0 = 4.33 ns and p'' = 200 mm. The parameters of the fitting are a_0 = −2.31E12, a_1 = 1.03E−4 s·rad^{-1}, a_2 = −1.56E−21 s^2·rad^{-2}, a_3 = 1.08E−38 s^3·rad^{-3}. The numerical values of GD(ω) are fitted for each S by the polynomial formula with a maximum error of about 12 as, see Fig. 7(a2). The very good fitting indicates that the assumption of a linear variation of the group delay with S at a fixed frequency is well verified.

The GDD is shown in Fig. 7(b). For S > 400 mm, it is always negative and the values are in agreement with what is required to compress the pulse as resulting from the generation modeling. The TOD is finally shown in Fig. 7(c). Note that the amount of the linear translation of G2 to finely tune the GDD is in the 5-10 mm range with a accuracy in the translation of the order of 0.5 mm. This gives a control of the delay of the order of 20 as.

#92254 - $15.00 USD Received 29 Jan 2008; revised 17 Mar 2008; accepted 21 Mar 2008; published 25 Apr 2008

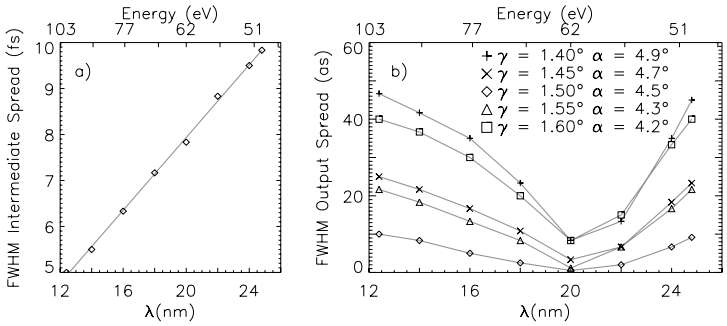

Fig. 5. Analysis of the time-delay compensation of the compressor for the 50-100 eV region. The graphs show the FWHM spreads of the optical paths of rays for different altitude angles on the gratings. For each altitude, the optimum azimuth is selected. a) Spread at the intermediate plane. The spreads are almost the same for different altitude angles. b) Spreads at the output plane.

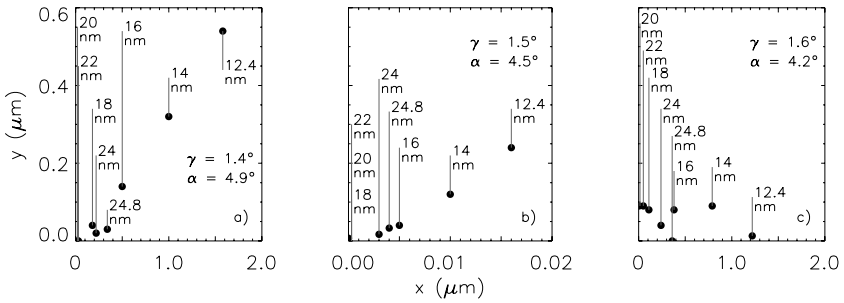

Fig. 6. Position of the spot size on the output focal plane for different altitude angles: a) γ = 1.4°, α = 4.9°; b) γ = 1.5°, α = 4.5°; c) γ = 1.6°, α = 4.2°. The best time-delay compensation (case b) is achieved when the spread of the focal positions is minimized.

5.3 Effect of the surface errors

The simulations have been performed in the case of ideal optical surfaces, i.e. with no figuring and no slope errors. Here, we analyze the degradation of the performances due to the non ideality of the surfaces, in particular we will distinguish between slope errors and figuring errors.

The slope errors are the high-frequency errors on the slope of the surface. State-of-the-art polishing on flat surfaces achieves around 1 μrad rms slope errors on mirrors of 1-m length. The errors are definitely smaller on small surfaces because the polishing process is more accurate. On a plane surface of size comparable to the size of the gratings of the compressor the typical values are about 0.5 μrad rms. On a small parabolic mirror the values are expected to be higher, about 1 μrad rms.

The system has been simulated including slope errors on each of the six surfaces to analyze the degradation on the time-delay compensation. The results are resumed in Fig. 8. In presence of slope errors, the spread of the optical paths increases to about 20 as FWHM. The phase properties are unchanged since they depend on the optical path made by the chief ray.

The figuring errors quantify the gap between the ideal surface and the actual one on the low-frequency scale. They are given in terms of fraction of the wavelength. Typical values on small surfaces are $\lambda/30$ (λ = 500 nm) and even lower for plane surfaces. These errors influence the optical performance of the instrument because they introduce aberrations that cannot be corrected. With the figuring errors that are normally achieved, the aberrations on the

#92254 - $15.00 USD Received 29 Jan 2008; revised 17 Mar 2008; accepted 21 Mar 2008; published 25 Apr 2008

output plane have been simulated to be in the range 1-2 μm and the time-delay compensation to be limited to 10-20 as FWHM.

It can be concluded that the temporal response of the instrument is limited to ≈20 as mainly by the quality achieved on the finishing of the optical surfaces.

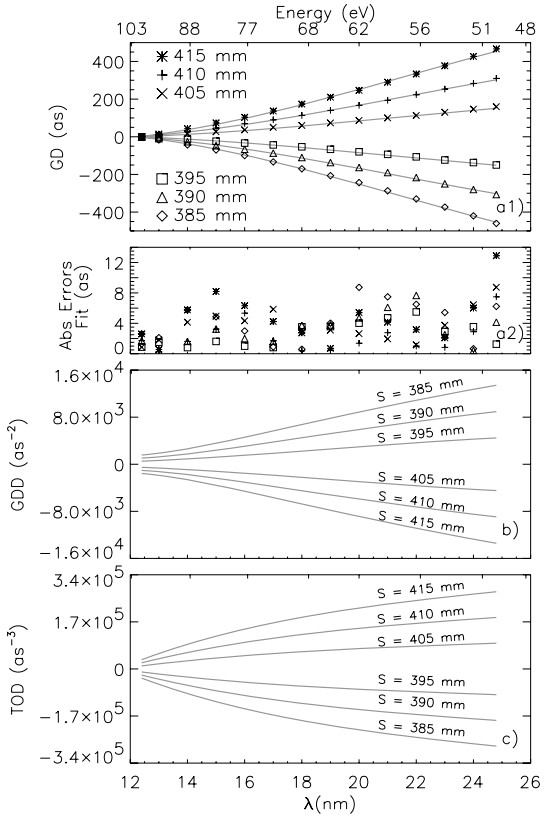

Fig. 7. Phase properties of the compressor in the 50-100 eV region. The group delay (a1), the error fit (a2), the GDD (b) and the TOD (c) are shown for different values of the parameter S.

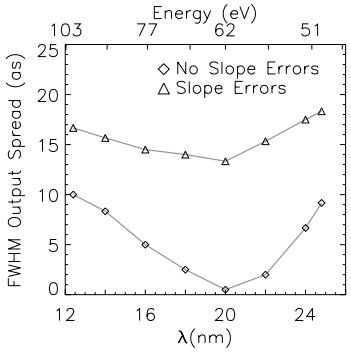

Fig. 8. Analysis of the time-delay compensation of the compressor for the 50-100 eV region with slope errors on the optics. The graphs show the FWHM spreads of the optical paths at the output. The slope errors are 1.0 μrad rms on the parabolic mirrors and 0.5 μrad rms on the plane gratings.

#92254 - $15.00 USD Received 29 Jan 2008; revised 17 Mar 2008; accepted 21 Mar 2008; published 25 Apr 2008

5.4 Beam stability

The XUV beam stability affects both the time-delay compensation and the phase properties of the compressor. In fact, any change on the direction of the input beam or in the position of the XUV source causes an increase of aberrations at the output plane and a variation of the lengths of the optical paths of the chief rays at the different wavelengths. Obviously, the XUV beam stability depends directly on the laser stability.

The effects of the beam instabilities on the performances have been simulated by the ray-tracing program. The requirements are given in terms of transverse stability, i.e. the spatial position of the attosecond XUV source, and angular stability, i.e. the direction of propagation of the attosecond XUV beam.

The requirements on the stability are given in terms of the maxima angular and spatial displacements that gives time-delay compensation within 30 as FWHM and variations of the length of the optical paths lower than 10 nm. The transverse stability has to be guaranteed within 0.2 mm and the pointing stability within 0.2° (3.5 mrad). These values are commonly achieved in laser systems for HH generation.

5.5 Use of toroidal mirrors

The use of parabolic mirrors on the configuration is required to reduce the aberrations of the optical configuration to negligible values. Since any aberration causes a spread of the optical paths, the managing of attosecond pulses requires a precise control of the aberrations that is made by using parabolic surfaces both to collimate the beam and to focus it.

The degradation of the performance due to the use of non ideal surfaces for the collimator and the focusing element is here explained. The same compressor that has been just analyzed is simulated by using four toroidal mirrors, as in the original TCM configuration [12]. The four mirrors have tangential and sagittal radii respectively equal to R = 7640 mm and ρ = 20.93 mm. All the parameters of the compressor remain unchanged as listed in Tab. 2.

The FWHM spread of the optical paths at the different wavelengths is shown in Fig. 9 for different acceptance angles. It is clear that even in the case of highly collimated beams, the time-delay compensation with toroidal mirrors is definitely worse than the case of parabolic mirrors. The spreads of the optical paths are of the order of few hundreds of attoseconds due to the residual aberrations in the output plane that are as high as 30 μm for the 6 mrad aperture. The TCM configuration with toroidal mirrors is well suited for time-delay compensation of femtosecond pulses but insufficient in the attosecond time scale.

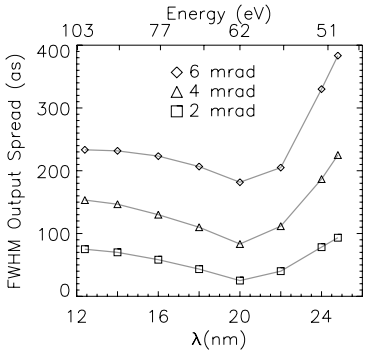

Fig. 9. Analysis of the time-delay compensation of the XAC for the 50-100 eV region with toroidal mirrors. The graph shows the FWHM spreads of the optical paths at the output for different acceptance angles. The parameters of the configurations are listed in Tab. 2.

#92254 - $15.00 USD Received 29 Jan 2008; revised 17 Mar 2008; accepted 21 Mar 2008; published 25 Apr 2008

6. Compressor for the 120-200 ev region

The power of an all-grazing-incidence design is the possibility of adopt the same configuration in any spectral region where the grazing-incidence optics can be used. In particular, the compressor scheme can be adopted for any region in the 4-100 nm interval having both high throughput and broad band of operation.

Here we briefly present the design of a compressor for the 120-200 eV (10.3-6.2 nm) interval. The optical parameters are reported in Tab. 3. The grazing angle on the mirrors has been decreased to 2.5° to maintain high reflectivity in the whole region of operation. The acceptance angle is 2 mrad that matches the expected divergence of ultrashort pulses in the high energy region. The gratings have 300 gr/mm groove density. They are blazed at 3.5° and are operated at an altitude of 1.2° to optimize the time-delay compensation.

As a coating, highly-dense graphite is considered as the most suitable for this spectral region. In fact, the reflectivity curve of conventional XUV metallic coatings operated at 2° grazing angle, such as Au or Pt, decreases from 0.94 at 10 nm to 0.73 at 6 nm, giving after four reflections a contribution to the total throughput that is not constant with the wavelength and rather poor especially at the lowest wavelengths, from 0.78 at 10 nm to 0.28 at 6 nm. Highly-dense graphite has higher reflectivity than conventional metallic coatings, especially for wavelengths lower than 10 nm, and is being currently adopted for mirrors for XUV free-electron-laser radiation, e.g. in the FLASH facility that is currently on operation at DESY Synchrotron [26]. The reflectivity of highly-dense graphite at 2° grazing angle in the 120-200 eV region is about 0.95 and almost constant with the wavelength, so the contribution of the mirrors to the total throughput is 0.80. The total transmission of the compressor, which includes also the efficiency of the gratings, is expected to be in the 0.15-0.20 range.

Since the size of the illuminated area of the optical elements is very small, the surface finishing is easily performed by the manufacturers with the high quality required for the operation with attosecond pulses. On such small areas, slope errors of less than 0.5 μrad rms and surface errors lower than $\lambda/40$ (λ = 500 nm) can be predicted.

Tab. 3. Parameters of the XAC for the 120-200 eV spectral region.

Pulse spectral interval	120-200 eV (10.3-6.2 nm)
Mirrors	**Paraboloidal**
Input/output arms	200 mm
Acceptance angle	2 mrad × 2 mrad
Grazing angle	2°
Size of illuminated area	12 mm × 0.4 mm
Coating	Highly dense graphite
Gratings	**Plane**
Groove density	300 gr/mm
Altitude angle	1.2°
Blaze angle	3.5°
Size of diffracting area	20 mm (// to the grooves) × 0.4 mm
Coating	Highly dense graphite
Distances	
S1, S2, S4	50 mm
S3	> 350 mm for negative GDD

As extensively discussed in the previous example, the parameters of the gratings have been selected to minimize the spread of the optical paths of rays at the same wavelengths within the angular aperture of the instrument. The time-delay compensation is almost perfect, with a residual spread of less than 15 as FWHM within the whole spectral region of operation. Due to the errors on the optical surfaces, the time-delay compensation is expected to be

#92254 - $15.00 USD Received 29 Jan 2008; revised 17 Mar 2008; accepted 21 Mar 2008; published 25 Apr 2008

limited to about 20 as. The phase properties of the compressor are resumed in Fig. 10. Even in this case the group delay has been obtained numerically by the ray-tracing program for different values of the distance S and then fitted by a 4th-order polynomial, which has been used to calculate the GDD and the TOD. The parameters of the fitting are a_0 = –9.60E11, a_1 = 2.31E–5 s·rad^{-1}, a_2 = –1.56E–22 s^2·rad^{-2}, a_3 = 5.471E–40 s^3·rad^{-3}. The numerical values of *GD*(ω) are fitted for each S by the polynomial formula with a maximum error of about 3 as.

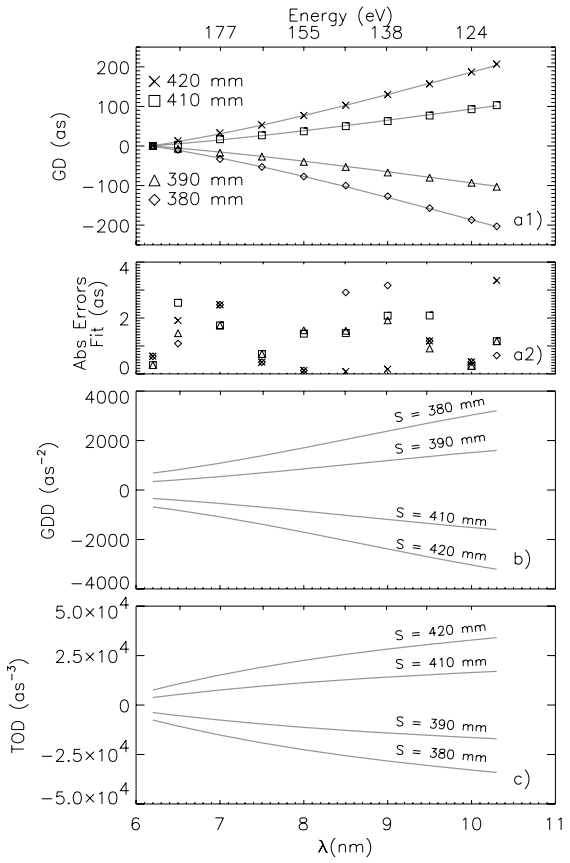

Fig. 10. Phase properties of the XAC in the 120-200 eV region. The group delay (a1), the error fit (a2), the GDD (b) and the TOD (c) are shown for different values of the parameter S.

7. Conclusions

We have here presented the optical design of a XUV double-grating compressor for broadband chirped attosecond pulses. The base of the design resides in the use of gratings in the off-plane mount, which gives much higher efficiency than the classical mount and excellent time-delay compensation in a wide spectral interval.

The scheme is very versatile: the compressor can be designed with high throughput in any spectral interval within the EUV region (4-100 nm). By a simple linear translation of a single grating, the instrument introduces a variable group delay in the range of few hundreds attoseconds with constant throughput and either negative or positive group-delay dispersion. The total efficiency is expected to be in the 0.15-0.20 range.

The extended spectral range of operation and the versatility in the control of the group delay allows the compression of XUV attosecond pulses beyond the limitations of the schemes based on metallic filters.

#92254 - $15.00 USD Received 29 Jan 2008; revised 17 Mar 2008; accepted 21 Mar 2008; published 25 Apr 2008